

The ^{103}Rh NMR Spectroscopy and Relaxometry of the Rhodium Formate Paddlewheel Complex

Harry Harbor Collins,¹ Mohamed Sabba,¹ Gamal Moustafa,¹ Bonifac Legrady,¹ Murari Soundararajan,¹ Markus Leutzsch,² and Malcolm H. Levitt¹

¹*School of Chemistry, University of Southampton, SO17 1BJ, UK*

²*Max-Planck-Institut für Kohlenforschung, Kaiser-Wilhelm-Platz 1, Mülheim an der Ruhr, 45470, Germany*

(*Electronic mail: mhl@soton.ac.uk)

(Dated: 25 July 2023)

The NMR spectroscopy of spin-1/2 nuclei with low gyromagnetic ratio is challenging, due to the low NMR signal strength. Methodology for the rapid acquisition of ^{103}Rh NMR parameters is demonstrated for the case of the rhodium formate “paddlewheel” complex $\text{Rh}_2(\text{HCO}_2)_4$. A scheme is described for enhancing the ^{103}Rh signal strength by polarization transfer from ^1H nuclei and which also greatly reduces the interference from ringing artifacts, a common hurdle for the direct observation of low- γ nuclei. The ^{103}Rh relaxation time constants T_1 and T_2 are measured within 20 minutes by using ^1H -detected experiments. The field-dependence of the ^{103}Rh T_1 is measured. The high-field relaxation is dominated by the chemical shift anisotropy (CSA) mechanism. The ^{103}Rh shielding anisotropy is found to be very large: $|\Delta\sigma| = 9900 \pm 540$ ppm. This estimate is compared with density functional theory calculations.

I. INTRODUCTION

Rhodium paddlewheel complexes have attracted significant attention due to their unique properties and diverse applications where they have played roles as catalysts and potential anticancer agents.^{1–5} These complexes consist of two rhodium atoms bridged by four carboxylate ligands, forming a lantern-like structure, with some resemblance to the paddlewheels of a river boat. A typical example is rhodium formate, $\text{Rh}_2(\text{HCO}_2)_4$, see figure 1.

Nuclear magnetic resonance (NMR) is a powerful probe of the properties of rhodium complexes. ^{103}Rh carries the distinction of being one of only 4 (with ^{19}F , ^{31}P , and ^{89}Y) spin-1/2 nuclei with a natural abundance of 100%. Nevertheless, it has been relatively neglected by spectroscopists: ^{103}Rh is a member of what Mann dubbed “the Cinderella nuclei”⁶ – transition metals with spin-1/2 but very low magnetogyric ratio γ . The NMR of ^{103}Rh is associated with multiple experimental challenges leading to a relative scarcity of experimental data. However, many of these challenges have been successfully overcome by the creative application of modern NMR methodology, such as heteronuclear multiple-quantum (HMQC) NMR⁷. However, although HMQC experiments allow the rapid acquisition of ^{103}Rh NMR spectra in suitable cases, it is not possible to estimate ^{103}Rh spin-lattice and spin-spin relaxation time constants through HMQC experiments. For this purpose, experiments exploiting ^{103}Rh magnetization are needed.

In this work, we utilise a variant of the PulsePol polarisation transfer technique^{8–10} to enhance the ^{103}Rh NMR spectroscopy of the rhodium formate paddlewheel complex in solution. We report (i) NMR methodology for the acquisition of directly detected ^{103}Rh spectra with effective ringing filtration; (ii) NMR methodology for the rapid measurement of ^{103}Rh T_1 and T_2 relaxation time constants over a range of magnetic field strengths. We observe a strong field dependence of the ^{103}Rh T_1 , which is qualitatively consistent with a dominant

chemical shift anisotropy relaxation mechanism. We estimate the ^{103}Rh shielding anisotropy by using information from ^{13}C and ^{103}Rh relaxation experiments in solution, and from ^{13}C solid-state NMR.

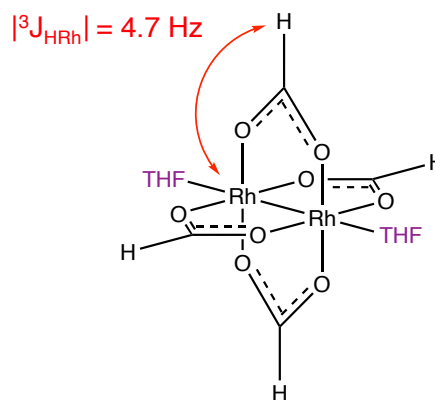


FIG. 1. Molecular structure of the rhodium formate paddlewheel complex ligated by solvent tetrahydrofuran (THF) molecules at the axial sites. This work exploits the $^3J_{\text{RhH}}$ scalar couplings for polarisation transfer between the ^{103}Rh and ^1H nuclei.

II. EXPERIMENTAL

A. Sample

Experiments were performed on a saturated (~ 10 mM) solution of rhodium formate ($\text{Rh}_2(\text{HCO}_2)_4$) dissolved in 500 μL deuterated tetrahydrofuran (THF-d_8) contained in a Wilmad LPV 5 mL sample tube. The rhodium formate was synthesised from rhodium chloride using a reported procedure¹¹ and dried extensively under heated vacuum. The

resulting rhodium formate solid was green in colour and dissolved in THF to produce a green solution.

B. Solution NMR

^1H and ^{103}Rh Spectra were acquired at a magnetic field strength of 9.4 T using a standard commercial Bruker 5 mm NMR BBO probe ($^1\text{H}/^2\text{H}/^{109}\text{Ag}-^{31}\text{P}$) equipped with a z-gradient with a maximum strength of 50 G cm^{-1} .

Proton resonances are referenced to the absolute frequency 400.14300 MHz; whereas ^{103}Rh resonances are referenced to an absolute frequency that is proportional to the protons ($\Xi(^{103}\text{Rh}) = 3.16\%$) per the most common convention¹².

Although the probe could be tuned to ^{103}Rh beyond the manufacturer specifications, it was set to mismatched (over-coupled) conditions to reduce ringdown times^{13–16}. The radiofrequency amplitudes on the ^1H and ^{103}Rh channels were both adjusted to give an intentionally matched nutation frequency of $\omega_{\text{nut}}/(2\pi) \simeq 4 \text{ kHz}$, corresponding to a 90° pulse duration of $62.5 \mu\text{s}$.

Additional isolation of the rf channels by electronic filters was found to be necessary - without the filters, noise on the ^{103}Rh channel was significant enough to preclude observation of other nuclei. At the preamplifier output we installed: a 30 MHz lowpass filter (Chemagnetics) on the ^{103}Rh channel, a 400 MHz bandpass filter (K&L Microwave) on the ^1H channel, and a 61 MHz bandpass filter (FSY Microwave) on the ^2H lock channel.

To measure relaxation times as a function of magnetic field, the experiments used rapid sample shuttling from inside the 9.4 T magnet bore to regions of lower field outside the magnet bore. The shuttling was performed using a motorised fast shuttling system based on the design by Kiryutin¹⁷. The shuttling time was kept constant at 1 second.

The pulse sequences described below use the following elements:

1. Composite pulses

Composite pulses were used to minimize the effects of rf field inhomogeneity and are denoted by shaded black rectangles in the pulse sequence diagrams. All composite pulses are implemented using the symmetrized BB1 composite pulse scheme^{18,19} in which a simple pulse β_ϕ (where β is the flip angle and ϕ is the phase) is replaced by:

$$(\beta/2)_\phi 180_{\phi+\theta_W} 360_{\phi+3\theta_W} 180_{\phi+\theta_W} (\beta/2)_\phi \quad (1)$$

Where $\theta_W = \arccos(-\beta/(4\pi))$. For the $\pi/2$ and π flip angles used in this paper, this corresponds to the following sequences:

$$90_\phi \rightarrow 45_\phi 180_{\phi+97.18} 360_{\phi+291.54} 180_{\phi+97.18} 45_\phi \quad (2)$$

$$180_\phi \rightarrow 90_\phi 180_{\phi+104.48} 360_{\phi+313.43} 180_{\phi+104.48} 90_\phi \quad (3)$$

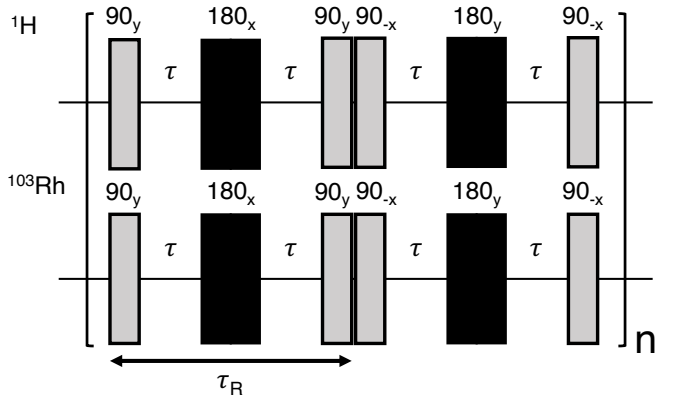


FIG. 2. DualPol pulse sequence used for ^1H - ^{103}Rh cross polarisation, and consisting of simultaneous PulsePol sequences⁸ on the two channels. Each PulsePol sequence is a repeating sequence of two R-elements. Each R-element has duration τ_R , and is given by a composite 180° pulse²⁰ with delays of duration τ between the pulses. The R-element duration should be short compared to the inverse of the relevant J-couplings. The black rectangles indicate BB1 composite π -pulses (equation 3).

2. DualPol Polarization Transfer Sequence

The transfer of polarisation between ^{103}Rh and ^1H was achieved using the pulse sequence shown in figure 2. This consists of repeating PulsePol sequences^{8,9}, applied simultaneously to the ^1H and ^{103}Rh radiofrequency channels. The PulsePol sequence consists of six phase-shifted radiofrequency pulses and four intervals τ , and was originally developed for polarization transfer between electron and nuclear spins in the context of nitrogen-vacancy diamond magnetometry⁸. It has also been shown to be effective for singlet-to-magnetization conversion^{9,10}, and has been interpreted in terms of symmetry-based recoupling theory¹⁰. For convenience, we refer to the "dual PulsePol" sequence in figure 2 as "DualPol".

DualPol is an unusual example of a solution-state polarization transfer sequence combining (i) multiple-pulse averaging^{21,22} and (ii) hard pulses separated by delays. The sequence provides robust polarization transfer even in the strong-coupling regime, where the standard INEPT sequence breaks down^{23–27}. That particular feature is not essential for the results described here. However, it is advantageous in other circumstances, as will be discussed in a future publication.

The repeating sequences of PulsePol and DualPol are composed of three-pulse elements of the form $90_y 180_x 90_{-x}$, with the pulses separated by intervals τ , and variants thereof. Each three-pulse sequence is therefore a "windowed" version of a composite 180° pulse²⁰. We therefore call this three-pulse sequence a "R-element", using notation originally introduced in the context of broadband heteronuclear decoupling²⁸, and later adapted for symmetry-based recoupling sequences in solid-state NMR²⁹, and symmetry-based singlet-triplet conversion sequences in solution NMR¹⁰. In the case of Du-

alPol, there is no special constraint or matching condition on the duration τ_R of the R-element, except that it should be much shorter than the period of the relevant J-coupling, $\tau_R \ll |^3J_{\text{RhH}}|^{-1}$. Under these conditions, the average Hamiltonian²¹ generated by the DualPol sequence, for a heteronuclear 2-spin system, has the form

$$\bar{H}^{(1)} \simeq \kappa_{\text{DP}} \times 2\pi J_{IS} (I_x S_x + I_y S_y) \quad (4)$$

where the nuclides ^1H and ^{103}Rh are referred to as I and S , respectively. The numbering convention for the average Hamiltonian terms starts with 1 for the lowest-order approximation, in common with the symmetry-based recoupling literature²⁹. The DualPol scaling factor is given, under suitable approximations, by $\kappa_{\text{DP}} \simeq \frac{1}{2}$ in the limit of strong radiofrequency pulses. Equation 4 corresponds to an anisotropic Hartmann-Hahn Hamiltonian³⁰, indicating that the DualPol sequence exchanges z -magnetization components between the I -spins and S -spins. The theory and performance of the DualPol sequence will be discussed in more depth in a future paper.

In the experiments described here, all DualPol sequences used an R-element duration of $\tau_R = 5$ ms and a repetition number of $n = 10$. The total duration of each DualPol sequence was $T = 2n\tau_R = 100$ ms.

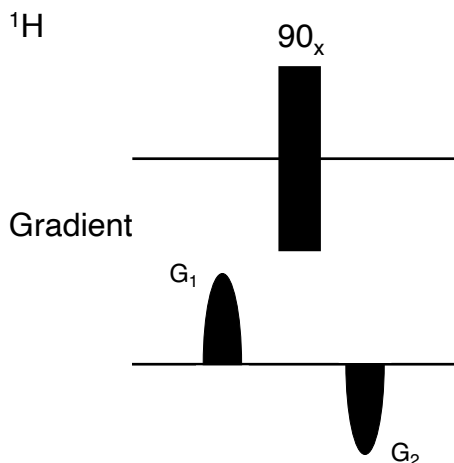


FIG. 3. Proton destruction filter for the removal of residual proton magnetisation. The gradient strengths are given by $G_1=100\%$ and $G_2=-61.8\%$ with respect to the maximum gradient strength 50 G cm^{-1} . Each gradient has a duration of 2 ms. The black rectangle indicates a BB1 composite $\pi/2$ pulse (equation 2).

3. ^1H Destruction Filter

The ^1H destruction filter is shown in figure 3. The filter has the net effect of dephasing residual proton transverse and longitudinal magnetisation (which may be generated by accidental excitation, and recovery during the decay interval respectively).

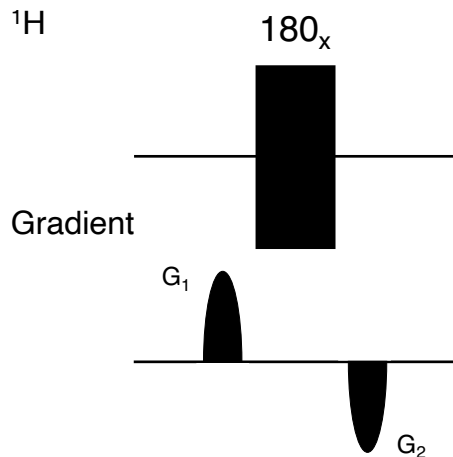


FIG. 4. Proton z-filter for the selection of proton z -magnetisation, using bipolar gradients. The gradient strengths are given by $G_1=40\%$ and $G_2=-40\%$ with respect to the maximum gradient strength of 50 G cm^{-1} . Each gradient pulse has a duration of 2 ms. The black rectangle indicates a BB1 composite π -pulse (equation 3).

4. ^1H z-filter

The z-filter for the selection of longitudinal ^1H magnetisation is shown in figure 4. This employs a bipolar gradient scheme in order to reduce spectral distortions by eddy currents or residual gradient fields³¹.

C. Solid-state NMR

Solid state CPMAS ^{13}C NMR was performed using a 4 mm Bruker probe at 14.1 T and ~ 303 K.

D. Computational Chemistry

Quantum chemical geometry optimisation and shielding tensor calculations for the rhodium formate complex axially ligated by solvent THF molecules were performed using the ORCA program package version 5.0.3³². ^{103}Rh shielding tensors were computed at the TPSSH/SARC-ZORA-TZVPP level of theory.

III. RESULTS

A. NMR Spectra

1. Solution-state ^1H Spectrum

The rhodium formate ^1H spectrum features a single formate ^1H resonance split into a 1:2:1 triplet by coupling to the pair of magnetically equivalent ^{103}Rh nuclei (figure 5). The three-bond ^1H - ^{103}Rh J-coupling is estimated to be $|^3J_{\text{RhH}}| = 4.7 \pm 0.1$ Hz.

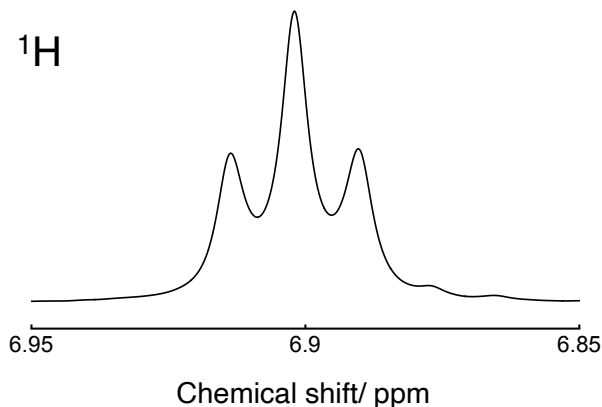


FIG. 5. ^1H spectrum of a ~ 10 mM solution of rhodium formate in THF-d_8 , acquired at 9.4 T and at 298 K in a single scan. Exponential line broadening (0.75 Hz) was applied.

2. Solution-state ^{103}Rh Spectra

The sequence shown in figure 6 was used for the acquisition of directly-detected ^{103}Rh spectra, enhanced by polarization transfer from ^1H nuclei. After an initial pair of 90° pulses, used for the suppression of ringing artefacts (see below), the DualPol sequence transfers z-magnetization from the ^1H to the ^{103}Rh nuclei, exploiting the form of the DualPol average Hamiltonian (equation 4). The resultant ^{103}Rh z-magnetization is converted into observable transverse magnetization by a final 90° pulse. The ^{103}Rh NMR signal is enhanced by a factor of up to $|\gamma/\gamma_S| \sim 31$, relative to that induced by a single 90° pulse applied to ^{103}Rh nuclei in thermal equilibrium.

Ringing artifacts are strongly suppressed by a phase-cycled pair of 90° pulses on the proton channel, before the polariza-

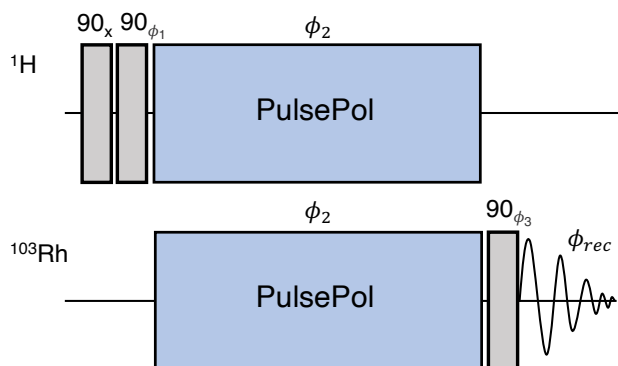


FIG. 6. Pulse sequence for the acquisition of ^1H enhanced ^{103}Rh spectra. A 16-step phase cycle is used where $\phi_1 = [-x, x, -x, x]$, $\phi_2 = [x, x, -x, -x]$, $\phi_3 = [x, x, x, x, y, y, y, y, -x, -x, -x, -x, -y, -y, -y, -y]$ and the receiver $\phi_{rec} = [x, -x, x, -x, y, -y, y, -y, -x, x, -x, x, -y, y, y]$ all of which combine to suppress ringing artefacts on the ^{103}Rh channel.

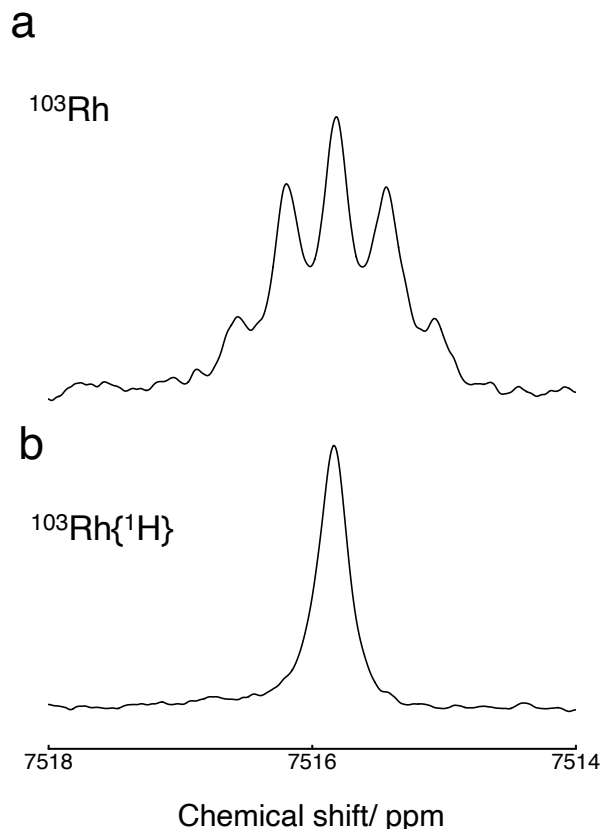


FIG. 7. (a) ^{103}Rh spectrum of a ~ 10 mM solution of rhodium formate in THF-d_8 scaled 2.5 times, acquired using 128 scans at 9.4 T and at 298 K using the pulse sequence in figure 6. (b) ^1H -decoupled ^{103}Rh spectrum acquired using 128 scans at 9.4 T and at 298 K using the pulse sequence in figure 6 with continuous-wave ^1H decoupling during signal acquisition. Acquisition time for each spectrum was 1 hour. Exponential line broadening (1 Hz) was applied to each spectrum.

tion transfer takes place. The signs of the ^1H magnetization and the ^{103}Rh receiver are simultaneously inverted in successive scans. Since the phases of the ringing are correlated with the phases of the pulses on the ^{103}Rh channel, the ringing is strongly suppressed in the ^{103}Rh spectrum. Further suppression of ringing is achieved by additional phase cycling of the PulsePol blocks. The sign of the ^{103}Rh magnetization is invariant under global phase shifts of the DualPol sequence, while the ringing contribution is phase-correlated and largely cancels out. Similar logic has been used to design excitation schemes for ringing suppression in homonuclear NMR experiments^{33,34}.

The rhodium formate ^{103}Rh spectrum features a single ^{103}Rh resonance split into a 1:4:6:4:1 pentet by couplings to the four equivalent ^1H nuclei on the formate ligands (figure 7(a)). The three-bond ^1H - ^{103}Rh J-coupling is estimated to be $|^3J_{\text{RhH}}| = 4.7 \pm 0.1$ Hz, in agreement with the ^1H spectrum. The ^{103}Rh resonances collapse into a single peak centred at 7516 ppm upon ^1H decoupling (figure 7(b)).

The ^{103}Rh resonances are broadened by the short ^{103}Rh T_2

(see figure-13).

The ^{103}Rh chemical shift is temperature-dependent (see Figure 8). The temperature-dependence of the ^{103}Rh chemical shift is approximately linear over the relevant temperature range, with a gradient of $\sim 1.48 \text{ ppm K}^{-1}$. This is in general agreement with observations on similar Rh complexes^{7,12}.

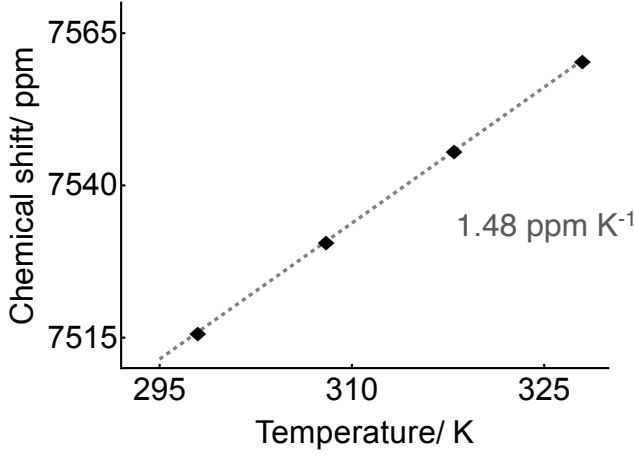


FIG. 8. ^{103}Rh chemical shift of rhodium formate dissolved in THF-d_8 at 9.4 T, as a function of temperature. The chemical shifts are referenced to $\Xi(^{103}\text{Rh}) = 3.16\%$.

3. Solid-state ^{13}C NMR

The chemical shift anisotropy (CSA) of the formate ^{13}C nuclei was estimated by magic-angle-spinning NMR experiments on rhodium formate solid (figure 9).

The estimated eigenvalues of the traceless, symmetric (rank-2) part of the shielding tensor are as follows: $\sigma_{xx}^{(2)} = 65.1 \text{ ppm}$, $\sigma_{yy}^{(2)} = 5.5 \text{ ppm}$, and $\sigma_{zz}^{(2)} = -70.7 \text{ ppm}$. This corresponds to the following Frobenius norm of the rank-2 ^{13}C shielding tensor:

$$\begin{aligned} \|\sigma^{(2)}\|(^{13}\text{C}) &= \{(\sigma_{xx}^{(2)})^2 + (\sigma_{yy}^{(2)})^2 + (\sigma_{zz}^{(2)})^2\}^{1/2} \\ &= 96.3 \pm 1.0 \text{ ppm} \end{aligned} \quad (5)$$

B. Relaxation Times

1. ^1H -Detected ^{103}Rh T_1

^{103}Rh T_1 relaxation time constants were measured indirectly through ^1H NMR signals using the sequence shown in figure 10. DualPol is used to transfer z-magnetization from the ^1H nuclei to the ^{103}Rh nuclei, and allowed to relax towards equilibrium during the relaxation interval τ_{relax} . For field-dependent relaxation measurements, the sample is shuttled to a region of lower magnetic field during this interval,

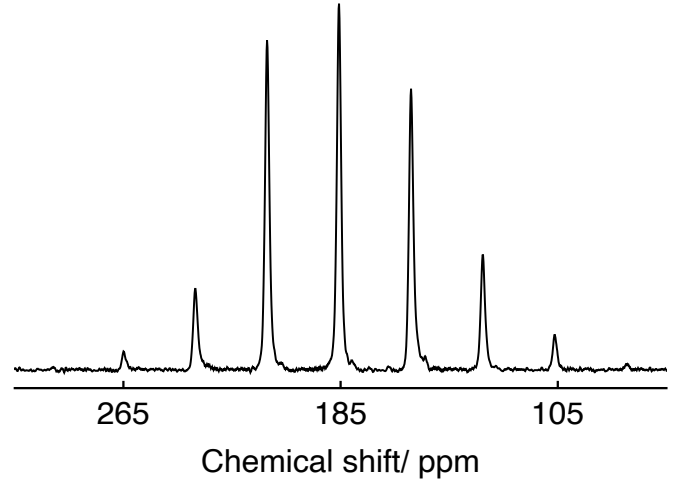


FIG. 9. Rhodium formate $^{13}\text{C}\{^1\text{H}\}$ solid-state CPMAS³⁵ NMR spectrum obtained at a spinning frequency of 4 kHz acquired using 2048 scans at 14.1 T and at 303K. The chemical shift was referenced to adamantane. The contact time was 160 μs . The recycle delay was 3 s. $\sim 150 \text{ mg}$ of sample was used. Further details of the pulse sequence are provided in the Supporting Information.

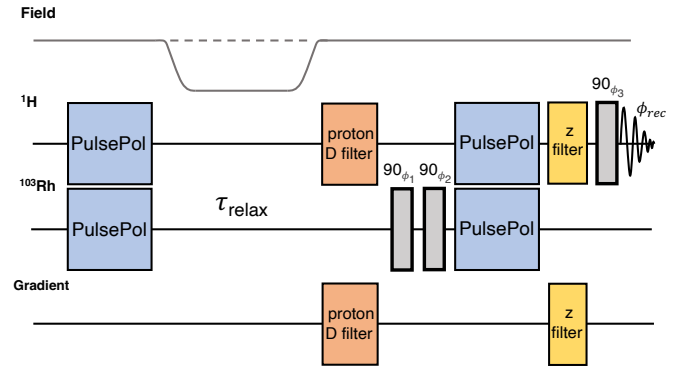


FIG. 10. Sequence used for the indirect measurement of rhodium T_1 through ^1H NMR signals. Phase cycles are given by $\phi_1 = [x, x, -x, -x]$, $\phi_2 = [-x, x, -x, x]$, $\phi_3 = [x, x, x, x, y, y, y, -x, -x, -x, -x, -y, -y, -y, -y]$ and the receiver $\phi_{\text{rec}} = [x, -x, -x, x, y, -y, -y, y, -x, x, x, -x, -y, y, y, -y]$. The optional shuttling of the sample to low field, and back again, during the interval τ_{relax} , is indicated.

and back again. A proton destruction filter is applied to eliminate any residual proton magnetisation, such as that generated during τ_{relax} through longitudinal relaxation towards equilibrium. Remaining ^{103}Rh z-magnetisation, selected for by the two 90° pulses, is now transferred back to ^1H z-magnetisation by a second DualPol block and is selected for by a proton z-filter. A final ^1H 90° pulse generates observable ^1H transverse magnetization. The sequence is repeated with variation of τ_{relax} in order to follow the equilibration of longitudinal ^{103}Rh magnetization.

The trajectory of indirectly-detected ^{103}Rh z-magnetization in a field of 9.4 T is shown in figure 11(a). The trajectory fits well to a single-exponential decay with time constant

$T_1(^{103}\text{Rh}) = 0.483 \pm 0.002$ s. A trajectory in the low magnetic field of 1 mT is shown in figure 11(b). This was produced by shuttling the sample to low magnetic field during the interval τ_{relax} . The relaxation process is much slower in low field, with a time constant of $T_1(^{103}\text{Rh}) = 28.2 \pm 1.2$ s.

The rhodium T_1^{-1} increases approximately quadratically with the magnetic field strength B , as shown in figure 11(c). The field-dependent relaxation rate constant is a reasonable fit to the quadratic function $T_1^{-1}(B) = T_1^{-1}(0) + aB^2$, where $T_1^{-1}(0) = 0.065 \pm 0.04 \text{ s}^{-1}$ and $a = 0.023 \pm 0.001 \text{ s}^{-1} \text{ T}^{-2}$.

2. ^1H -Detected ^{103}Rh T_2

The sequence shown in figure 12 was used to measure the ^{103}Rh spin-spin relaxation time constant T_2 in high magnetic field.

Conversion of ^1H z-polarization to ^{103}Rh z-polarization is achieved via DualPol. ^{103}Rh transverse magnetisation is generated by a 90° pulse and allowed to decay during the subsequent spin echo of duration τ_{echo} . The ensuing 90° ^{103}Rh pulse returns the remaining transverse ^{103}Rh magnetisation back to longitudinal ^{103}Rh polarisation. A ^1H destruction filter destroys any residual ^1H magnetisation before another DualPol cross-polarisation block transfers ^{103}Rh z-magnetisation back to ^1H z-magnetization. The ^1H z-filter selects for ^1H z-magnetization before the ^1H signal is induced by the final 90° ^1H pulse. The pulse sequence is repeated varying the echo delay τ_{echo} in order to follow the decay of ^{103}Rh transverse magnetization.

The trajectory of indirectly-detected ^{103}Rh transverse magnetization in a field of 9.4 T is shown in figure 13. The trajectory fits well to a single-exponential decay with time constant $T_2(^{103}\text{Rh}) = 0.181 \pm 0.001$ s. Note that the measured value of T_2 is much smaller than T_1 under the same conditions.

3. ^{13}C inversion-recovery

As discussed below, the rotational correlation time τ_c of the rhodium formate complex may be estimated by a study of the ^{13}C longitudinal relaxation. This data was obtained by an indirect detection method exploiting the scalar-coupled formate protons, as described in the Supporting Information. The inversion-recovery data fits well to a single-exponential recovery with a time constant of 2.64 ± 0.13 s for a solution in THF- d_8 , in a magnetic field of 9.4 T. However, as described below, the inversion-recovery curve for the ^{13}C magnetization is best analyzed using a bi-exponential relaxation model.

IV. DISCUSSION

As shown in figure 11(c), the ^{103}Rh relaxation rate constant T_1^{-1} has a quadratic dependence on magnetic field B , with an additional zero-field contribution of $T_1^{-1}(0) = 0.0653 \pm 0.0383 \text{ s}^{-1}$. The quadratic field dependence is consistent

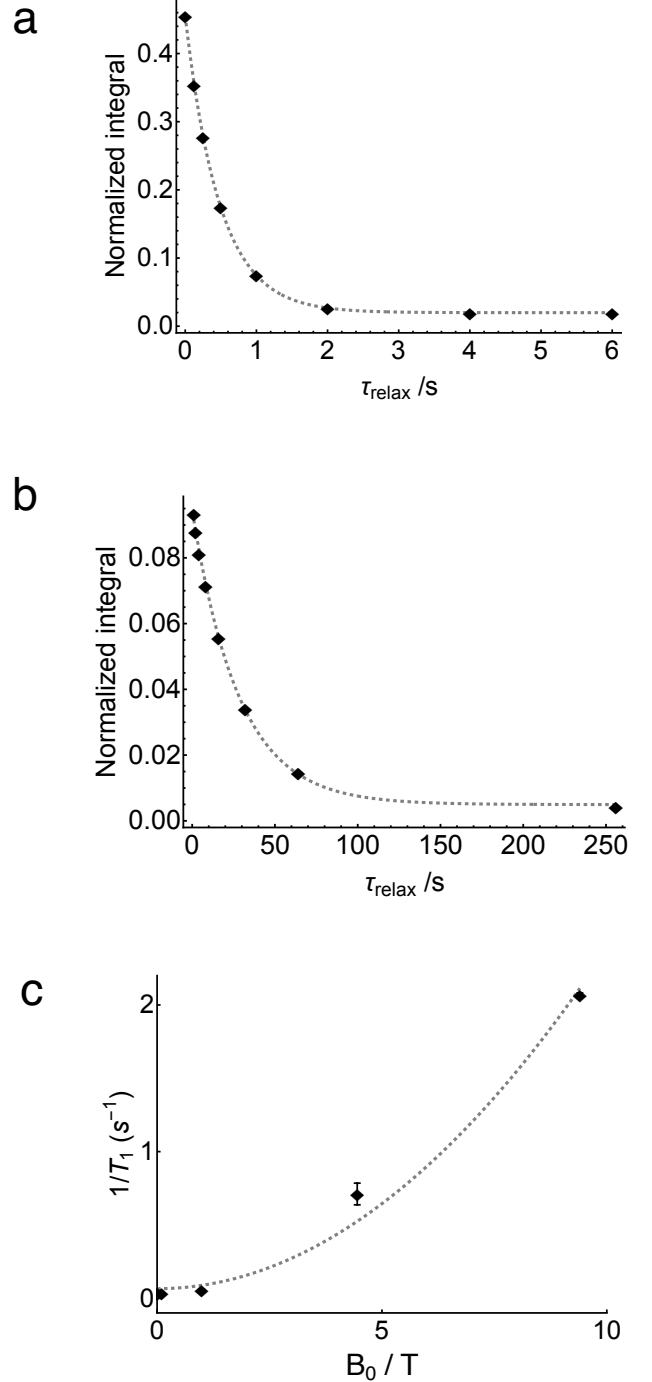


FIG. 11. (a) Decay curve for ^{103}Rh longitudinal magnetization at a field of 9.4 T, obtained using the pulse sequence in figure 10, but without shuttling the sample to low field. The data was acquired in ~ 20 minutes. The integrals are normalised against the ^1H spectrum obtained by a single ^1H 90° pulse applied to a system in thermal equilibrium at 9.4 T. The data fits well to an exponential decay with time constant $T_1 = 0.483 \pm 0.002$ s. (b) Decay curve for ^{103}Rh longitudinal magnetization at a field of 1 mT, obtained using the pulse sequence in figure 10, including the shuttling of the sample to low field. The data fits well to an exponential decay with time constant $T_1 = 28.2 \pm 1.2$ s. (c) ^{103}Rh relaxation rate constant T_1^{-1} as a function of magnetic field strength. The dashed line shows the quadratic function $T_1^{-1}(B) = T_1^{-1}(0) + aB^2$, where $T_1^{-1}(0) = 0.065 \pm 0.038 \text{ s}^{-1}$ and $a = 0.023 \pm 0.001 \text{ s}^{-1} \text{ T}^{-2}$.

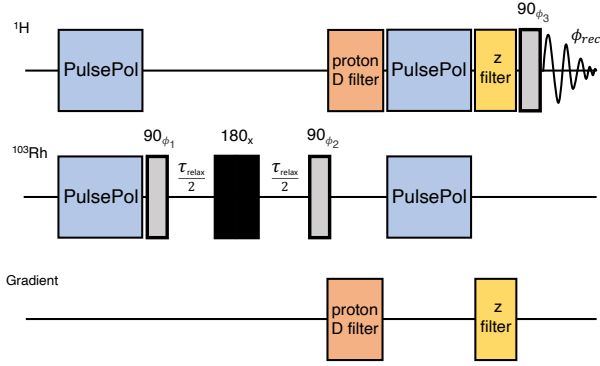


FIG. 12. Sequence used for the indirect measurement of rhodium T_2 with detection on protons. Phase cycles are given by $\phi_1 = [x, x, -x, -x]$, $\phi_2 = [-x, x, -x, x]$, $\phi_3 = [x, x, x, x, y, y, y, y, -x, -x, -x, -x, -y, -y, -y, -y]$ and the receiver $\phi_{rec} = [x, -x, -x, x, y, -y, y, -y, -x, x, x, -x, -y, y, y, -y]$. The black rectangle indicates a BB1 composite π -pulse (equation 3).

with a dominant chemical shift anisotropy (CSA) relaxation mechanism, as is commonly observed for the ^{103}Rh NMR of rhodium complexes^{12,36}.

It is difficult to estimate the ^{103}Rh chemical shift anisotropy by solid-state NMR. The small magnetogyric ratio of ^{103}Rh and the very large CSA value make solid-state ^{103}Rh NMR very difficult. Our attempts to use the PROSPR method³⁷ to observe the ^{103}Rh spectrum indirectly in the solid state, by saturation transfer to the ^1H nuclei, were also unsuccessful. This is likely due to the very small dipole-dipole couplings between ^1H and ^{103}Rh nuclei in this complex, which greatly inhibits dipolar-mediated polarization transfer in the solid state.

The symmetry of the complex indicates that the ^{103}Rh CSA tensors should have uniaxial symmetry ($\eta = 0$) with their

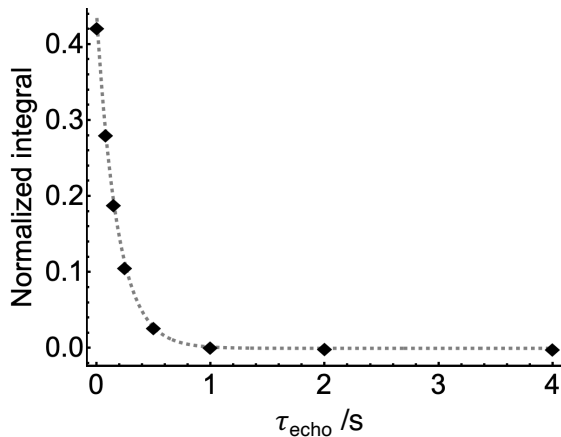


FIG. 13. Decay curve for ^{103}Rh transverse magnetization at a field of 9.4 T, obtained using the pulse sequence in figure 12. The data fits well to an exponential decay with time constant $T_2 = 0.181 \pm 0.001$ s. The integrals are normalised against the ^1H spectrum obtained by a single ^1H 90° pulse applied to a system in thermal equilibrium at 9.4 T.

unique principal axis along the Rh-Rh bond. This property is assumed in the following discussion.

Although the ^{103}Rh CSA may not be measured directly, it is possible to estimate it by a combination of field-dependent ^{103}Rh and ^{13}C T_1 measurements. The compact cage structure of the rhodium formate complex (figure 1) suggests that, to a good approximation, the complex tumbles in solution as a near-rigid body, with a common rotational correlation time τ_c for all spin interactions. This approximation allows a correlation time estimate from ^{13}C NMR to be applied in the context of ^{103}Rh NMR.

A ^{13}C nucleus of rhodium formate experiences two strong anisotropic interactions: the ^{13}C - ^1H dipole-dipole coupling with the directly-bonded hydrogen nucleus, and the ^{13}C chemical shift anisotropy. For point nuclei (i.e. ignoring the spatial spread of the nuclear wavefunctions), the ^{13}C - ^1H dipole-dipole coupling constant is given by $b_{CH} = -(\mu_0/4\pi)\hbar\gamma_C\gamma_H r_{CH}^{-3}$, where r_{CH} is the ^{13}C - ^1H internuclear distance³⁸. Quantum chemical calculations³² (see SI) predict an internuclear ^{13}C - ^1H distance of 1.097 Å, corresponding to a dipole-dipole coupling constant of $b_{CH} = -2\pi \times 22.8$ kHz. However, solid-state NMR studies have shown that the true dipole-dipole coupling is weakened by the angular spread of the ^1H wavefunctions, associated with the zero-point librational motion of the C-H bonds³⁹. In the calculations below, we therefore assume a ^{13}C - ^1H dipole-dipole coupling constant of $b_{CH} = -2\pi \times (20.4 \pm 0.5)$ kHz.

For isolated ^{13}C - ^1H spin systems in the extreme narrowing approximation (fast tumbling), the theoretical recovery of ^{13}C longitudinal magnetization $M_z(t)$ after perturbation from equilibrium at time $t = 0$ is expected to follow the biexponential curve

$$M_z(t) = M_z^{\text{eq}} + (M_z(0) - M_z^{\text{eq}}) \times \frac{1}{2} \left(\exp\left\{-\left(\frac{1}{2}b_{CH}^2 + \frac{1}{5}\omega_{\text{CSA}}^2\right)\tau_c\right\} + \exp\left\{-\left(\frac{3}{2}b_{CH}^2 + \frac{1}{5}\omega_{\text{CSA}}^2\right)\tau_c\right\} \right) \quad (6)$$

where M_z^{eq} is the thermal equilibrium ^{13}C magnetization, and ω_{CSA} is defined as follows:

$$\omega_{\text{CSA}} = -\gamma_C B^0 \|\sigma^{(2)}\| \quad (7)$$

where $\|\sigma^{(2)}\|$ is the norm of the ^{13}C shielding tensor, as defined in equation 5. The biexponential form of equation 6 is due to ^1H - ^{13}C cross-relaxation during the magnetization recovery^{40–42}.

In a magnetic field of 9.4 T, the ^{13}C CSA, as estimated by ^{13}C solid-state NMR (section III A 3), corresponds to an interaction strength of $\omega_{\text{CSA}} \simeq 2\pi \times (9.7 \pm 0.1)$ kHz. By fitting the experimental ^{13}C inversion-recovery trajectory to an equation of the form in eq. 6, we obtain the following estimate of the rotational correlation time for the rhodium formate paddlewheel complex in THF- d_8 solution at 298 K: $\tau_c \simeq 24.5 \pm 1.5$ ps. The ^{103}Rh relaxation may now be analyzed using the estimate of τ_c from the ^{13}C data. As shown in figure 11, the ^{103}Rh T_1^{-1} relaxation rate constant is well-described by the function $T_1^{-1}(B) = T_1^{-1}(0) + aB^2$, with the field-independent

term $T_1^{-1}(0) = 0.065 \pm 0.038 \text{ s}^{-1}$, and the quadratic coefficient $a = 0.023 \pm 0.001 \text{ s}^{-1} \text{ T}^{-2}$.

The quadratic field-dependent term may be ascribed to the CSA mechanism. In the extreme narrowing approximation (fast tumbling), the CSA contribution to the T_1^{-1} relaxation rate constant for ^{103}Rh is given by⁴²

$$(T_1(^{103}\text{Rh}))_{\text{CSA}}^{-1} = \frac{2}{15} B_0^2 \gamma_{\text{Rh}}^2 \Delta\sigma^2 \tau_c \quad (8)$$

where the shielding anisotropy $\Delta\sigma$ is defined as follows⁴²:

$$\Delta\sigma = \frac{3}{2}(\sigma_{\text{ZZ}} - \sigma_{\text{iso}}) = -\frac{3}{2}\delta^{\text{aniso}} \quad (9)$$

Equation 8 implies that the quadratic field-dependent coefficient a for the ^{103}Rh T_1^{-1} relaxation rate constant is given by

$$a = \frac{2}{15} \gamma_{\text{Rh}}^2 \Delta\sigma^2 \tau_c \quad (10)$$

The experimental estimate of the quadratic coefficient $a = 0.023 \pm 0.001 \text{ s}^{-1} \text{ T}^{-2}$ may be combined with the correlation time estimate $\tau_c \simeq 24.5 \pm 1.5 \text{ ps}$ to obtain the following experimental estimate of the ^{103}Rh shielding anisotropy: $|\Delta\sigma| = 9900 \pm 540 \text{ ppm}$.

This is a very large number. Although prior estimates of the ^{103}Rh CSA are scarce in the literature, CSA values for heavy spin-1/2 nuclei are sometimes of a similar magnitude^{43–52}, with closely related platinum (II) compounds displaying ^{195}Pt CSA values on the order of 10,000 ppm^{43,45,50,52}. To our knowledge, the only other measurements of ^{103}Rh CSAs, in very different Rh(III) compounds, were on the order of ~ 500 –1500 ppm^{53,54}. This dramatic range is also typical^{46,47,51} for heavy spin-1/2 nuclei.

Using ORCA^{32,55,56}, ^{103}Rh shielding tensors were computed at the TPSSH/SARC-ZORA-TZVPP level of theory using implicit solvation (CPCM^{57,58} for THF), the zeroth-order regular approximation (ZORA)^{59,60} for the inclusion of relativistic effects, GIAOs, the RI approximation⁵⁶, and the tau-dependent correction as suggested by Dobson^{61–63} (see Supporting Information). The result is summarised in table I.

The calculated CSA is somewhat smaller than the experimental estimate. Underestimation of CSAs calculated using the ZORA method has been reported for other heavy spin-1/2 nuclei^{64–66}, where better agreement might be obtained with higher-order four-component relativistic calculations⁶⁵ or by accounting for the relativistic breakdown of the relationship between spin-rotation and the paramagnetic contribution to the anisotropy⁶⁶.

The origin of the zero-field contribution $T_1^{-1}(0)$ to the ^{103}Rh relaxation rate constant is currently unknown. As discussed in the Supporting Information, the ^{103}Rh - ^{103}Rh and ^{103}Rh - ^1H dipole-dipole couplings are much too weak to account for this term. In the literature, the low-field relaxation of heavy spin-1/2 nuclei is often attributed to a spin-rotation mechanism. However, to our knowledge, this conclusion has not been supported by any theoretical or computational studies.

Method	$ \Delta\sigma $ /ppm
Calculated	7070
Experimental estimate	9900 ± 540

TABLE I. Estimates of the ^{103}Rh shielding tensor anisotropy $\Delta\sigma$ of Rh formate, defined in equation 9. The computational estimate is given by quantum chemical calculation using ORCA³². The experimental estimate is from the analysis of field-dependent ^{103}Rh relaxation in solution, as described in this paper.

The experimental estimate of the ^{103}Rh T_2 is much shorter than the estimate of T_1 under the same conditions ($T_2 = 0.181 \pm 0.001 \text{ s}$ as against $T_1 = 0.483 \pm 0.002 \text{ s}$, in a field of 9.4 T. We tentatively attribute the short T_2 value to the modulation of the isotropic chemical shift by ligand exchange at the axial positions. Other decoherence mechanisms, such as diffusion in the presence of inhomogeneous magnetic fields, are expected to be too weak to account for the observed T_2 value in this case.

In conclusion, this paper has demonstrated methodology for the indirect estimation of ^{103}Rh T_1 and T_2 values by magnetization transfer to and from ^1H nuclei using the DualPol pulse sequence. Field-dependent ^{103}Rh T_1 measurements indicate a very large chemical shift anisotropy for the ^{103}Rh sites in the rhodium formate paddlewheel complex. The field-independent contribution to the ^{103}Rh relaxation rate constant is not fully understood at the current time.

A limitation of the methodology described here is the prerequisite of a spin system with direct scalar couplings between ^{103}Rh nuclei and a proton, which is not present in all rhodium complexes. This limitation may be addressed via the use of a relay nucleus, such as ^{13}C at natural abundance.^{7,67–69}

ACKNOWLEDGMENTS

We acknowledge funding from the European Research Council (grant 786707-FunMagResBeacons), and EPSRC-UK (grants EP/P009980/1, EP/P030491/1, EP/V055593/1). M.L. acknowledges financial support by the Max-Planck-Gesellschaft and the Max-Planck-Institut für Kohlenforschung. We thank Alexander A. Auer for advice on quantum chemical calculations. We thank Professor Brian E. Mann for advice and historical insights on rhodium NMR. We thank Alexey Kiryutin for sharing his designs for the sample shuttle.

AUTHOR DECLARATIONS

Conflict of interest

The authors have no conflicts to disclose.

DATA AVAILABILITY STATEMENT

The data that support the findings of this study are available from the corresponding author upon reasonable request.

- ¹A. Erck, L. Rainen, J. Whyleyman, I.-M. Chang, A. P. Kimball, and J. Bear, "Studies of Rhodium(II) Carboxylates as Potential Antitumor Agents," *Proceedings of the Society for Experimental Biology and Medicine* **145**, 1278–1283 (1974).
- ²M. Fandzloch, A. W. Augustyniak, L. Dobrzańska, T. Jędrzejewski, J. Sitkowski, M. Wypij, and P. Golińska, "First dinuclear rhodium(II) complexes with triazolopyrimidines and the prospect of their potential biological use," *Journal of Inorganic Biochemistry* **210**, 111072 (2020).
- ³J. Ohata and Z. T. Ball, "Rhodium at the chemistry–biology interface," *Dalton Transactions* **47**, 14855–14860 (2018).
- ⁴S. Lin and C. Turro, "Dirhodium Complexes as Panchromatic Sensitizers, Electrocatalysts, and Photocatalysts," *Chemistry – A European Journal* **27**, 5379–5387 (2021).
- ⁵R. Hrdina, "Dirhodium(II,II) Paddlewheel Complexes," *European Journal of Inorganic Chemistry* **2021**, 501–528 (2021).
- ⁶B. E. Mann, "The Cinderella Nuclei," in *Annual Reports on NMR Spectroscopy*, Vol. 23, edited by G. A. Webb (Academic Press, 1991) pp. 141–207.
- ⁷F. P. Caló, G. Bistoni, A. A. Auer, M. Leutzsch, and A. Fürstner, "Triple Resonance Experiments for the Rapid Detection of ¹⁰³Rh NMR Shifts: A Combined Experimental and Theoretical Study into Dirhodium and Bismuth–Rhodium Paddlewheel Complexes," *Journal of the American Chemical Society* **143**, 12473–12479 (2021).
- ⁸I. Schwartz, J. Scheuer, B. Tratzmiller, S. Müller, Q. Chen, I. Dhand, Z.-Y. Wang, C. Müller, B. Naydenov, F. Jelezko, and M. B. Plenio, "Robust optical polarization of nuclear spin baths using Hamiltonian engineering of nitrogen-vacancy center quantum dynamics," *Science Advances* **4** (2018), 10.1126/sciadv.aat8978.
- ⁹B. Tratzmiller, *Pulsed Control Methods with Applications to Nuclear Hyperpolarization and Nanoscale NMR*, Ph.D. thesis, Universität Ulm (2021).
- ¹⁰M. Sabba, N. Wili, C. Bengs, J. W. Whiphham, L. J. Brown, and M. H. Levitt, "Symmetry-based singlet-triplet excitation in solution nuclear magnetic resonance," *The Journal of Chemical Physics* **157**, 134302 (2022).
- ¹¹G. A. Rempel, P. Legzdins, H. Smith, G. Wilkinson, and D. A. Ucko, "Tetrakis(acetato)dirhodium(II) and Similar Carboxylato Compounds," in *Inorganic Syntheses* (John Wiley & Sons, Ltd, 1972) pp. 90–91.
- ¹²L. Carlton, "Chapter 3 - Rhodium-103 NMR," in *Annual Reports on NMR Spectroscopy*, Vol. 63, edited by G. A. Webb (Academic Press, 2008) pp. 49–178.
- ¹³G. C. Chingas, "Overcoupling NMR probes to improve transient response," *Journal of Magnetic Resonance* **54**, 153–157 (1983).
- ¹⁴M. L. Buess and G. L. Petersen, "Acoustic ringing effects in pulsed nuclear magnetic resonance probes," *Review of Scientific Instruments* **49**, 1151–1155 (1978).
- ¹⁵I. P. Gerothanassis, "Methods of avoiding the effects of acoustic ringing in pulsed fourier transform nuclear magnetic resonance spectroscopy," *Progress in Nuclear Magnetic Resonance Spectroscopy* **19**, 267–329 (1987).
- ¹⁶E. Fukushima and S. B. W. Roeder, "Spurious ringing in pulse NMR," *Journal of Magnetic Resonance* **33**, 199–203 (1979).
- ¹⁷A. S. Kiryutin, A. N. Pravdivtsev, K. L. Ivanov, Y. A. Grishin, H.-M. Vieth, and A. V. Yurkovskaya, "A fast field-cycling device for high-resolution NMR: Design and application to spin relaxation and hyperpolarization experiments," *Journal of Magnetic Resonance* **263**, 79–91 (2016).
- ¹⁸S. Wimperis, "Broadband, Narrowband, and Passband Composite Pulses for Use in Advanced NMR Experiments," *Journal of Magnetic Resonance, Series A* **109**, 221–231 (1994).
- ¹⁹H. K. Cummins, G. Llewellyn, and J. A. Jones, "Tackling systematic errors in quantum logic gates with composite rotations," *Physical Review A* **67**, 042308 (2003).
- ²⁰M. H. Levitt and R. Freeman, "NMR population inversion using a composite pulse," *Journal of Magnetic Resonance* **33**, 473–476 (1979).
- ²¹U. Haeberlen and J. S. Waugh, "Coherent Averaging Effects in Magnetic Resonance," *Physical Review* **175**, 453–467 (1968).
- ²²E. R. P. Zuiderweg, "Analysis of multiple-pulse-based heteronuclear J cross polarization in liquids," *Journal of Magnetic Resonance* **89**, 533–542 (1990).
- ²³B. Baishya and C. L. Khetrapal, "Perfect echo" INEPT: More efficient heteronuclear polarization transfer by refocusing homonuclear J-coupling interaction," *Journal of Magnetic Resonance* **242**, 143–154 (2014).
- ²⁴R. T. Williamson, B. L. Márquez, W. H. Gerwick, and K. E. Kövér, "One- and two-dimensional gradient-selected HSQMB NMR experiments for the efficient analysis of long-range heteronuclear coupling constants," *Magnetic Resonance in Chemistry* **38**, 265–273 (2000).
- ²⁵H. Koskela, I. Kilpeläinen, and S. Heikkinen, "Some aspects of quantitative 2D NMR," *Journal of Magnetic Resonance* **174**, 237–244 (2005).
- ²⁶S. Gil, J. F. Espinosa, and T. Parella, "Accurate measurement of small heteronuclear coupling constants from pure-phase α/β HSQMB cross-peaks," *Journal of Magnetic Resonance* **213**, 145–150 (2011).
- ²⁷H. Koskela, I. Kilpeläinen, and S. Heikkinen, "LR-CAHSQC: An application of a Carr–Purcell–Meiboom–Gill-type sequence to heteronuclear multiple bond correlation spectroscopy," *Journal of Magnetic Resonance* **164**, 228–232 (2003).
- ²⁸M. H. Levitt and R. Freeman, "Composite pulse decoupling," *Journal of Magnetic Resonance* **43**, 502–507 (1981).
- ²⁹M. Carravetta, M. Edén, X. Zhao, A. Brinkmann, and M. H. Levitt, "Symmetry principles for the design of radiofrequency pulse sequences in the nuclear magnetic resonance of rotating solids," *Chemical Physics Letters* **321**, 205–215 (2000).
- ³⁰S. J. Glaser and J. J. Quant, "Homonuclear and Heteronuclear Hartmann–Hahn Transfer in Isotropic Liquids," in *Advances in Magnetic and Optical Resonance*, Vol. 19, edited by W. S. Warren (Academic Press, 1996) pp. 59–254e.
- ³¹G. Wider, V. Dotsch, and K. Wuthrich, "Self-Compensating Pulsed Magnetic-Field Gradients for Short Recovery Times," *Journal of Magnetic Resonance, Series A* **108**, 255–258 (1994).
- ³²F. Neese, F. Wennmohs, U. Becker, and C. Riplinger, "The ORCA quantum chemistry program package," *The Journal of Chemical Physics* **152**, 224108 (2020).
- ³³S. Zhang, X. Wu, and M. Mehring, "Elimination of ringing effects in multiple-pulse sequences," *Chemical Physics Letters* **173**, 481–484 (1990).
- ³⁴F. Wang, S. K. Ramakrishna, P. Sun, and R. Fu, "Triple-pulse excitation: An efficient way for suppressing background signals and eliminating radio-frequency acoustic ringing in direct polarization NMR experiments," *Journal of Magnetic Resonance* **332**, 107067 (2021).
- ³⁵B. H. Meier, "Cross polarization under fast magic angle spinning: Thermodynamical considerations," *Chemical Physics Letters* **188**, 201–207 (1992).
- ³⁶M. Cocivera, G. Ferguson, R. E. Lenkinski, P. Szczecinski, F. J. Lalor, and D. J. O'Sullivan, "NMR relaxation studies of ¹⁰³Rh," *Journal of Magnetic Resonance* **46**, 168–171 (1982).
- ³⁷M. J. Jarnoszewicz, A. R. Altenhof, R. W. Schurko, and L. Frydman, "Sensitivity Enhancement by Progressive Saturation of the Proton Reservoir: A Solid-State NMR Analogue of Chemical Exchange Saturation Transfer," *Journal of the American Chemical Society* **143**, 19778–19784 (2021).
- ³⁸M. H. Levitt, *Spin Dynamics. Basics of Nuclear Magnetic Resonance*, 2nd ed. (Wiley, Chichester, 2007).
- ³⁹T. Nakai, J. Ashida, and T. Terao, "Influence of small-amplitude motions on two-dimensional N.M.R. powder patterns," *Molecular Physics* **67**, 839–847 (1989).
- ⁴⁰I. Solomon, "Relaxation Processes in a System of Two Spins," *Physical Review* **99**, 559–565 (1955).
- ⁴¹T. D. Alger, R. Freeman, and D. M. Grant, "Carbon-13 T1 Measurements under Proton Coupled and Decoupled Conditions," *The Journal of Chemical Physics* **57**, 2168–2171 (1972).
- ⁴²J. Kowalewski and L. Mäler, *Nuclear Spin Relaxation in Liquids Theory, Experiments, and Applications*, 2nd ed. (CRC Press, Taylor & Francis Group, Boca Raton, FL, 2018).
- ⁴³J. J. Dechter and J. Kowalewski, "195Pt spin-lattice relaxation and shielding anisotropy for Pt(acac)₂," *Journal of Magnetic Resonance* **59**, 146–149 (1984).
- ⁴⁴P. Paluch, A. G. M. Rankin, J. Trébosc, O. Lafon, and J.-P. Amoureux, "Analysis of HMQC experiments applied to a spin $\frac{1}{2}$ nucleus subject to very large CSA," *Solid State Nuclear Magnetic Resonance* **100**, 11–25 (2019).

- ⁴⁵S. W. Sparks and P. D. Ellis, "Platinum-195 shielding tensors in potassium hexachloroplatinate(IV) and potassium tetrachloroplatinate(II)," *Journal of the American Chemical Society* **108**, 3215–3218 (1986).
- ⁴⁶A. Venkatesh, A. Lund, L. Rochlitz, R. Jabbour, C. P. Gordon, G. Menzildjian, J. Viger-Gravel, P. Berruyer, D. Gajan, C. Cop  ret, A. Lesage, and A. J. Rossini, "The Structure of Molecular and Surface Platinum Sites Determined by DNP-SENS and Fast MAS 195Pt Solid-State NMR Spectroscopy," *Journal of the American Chemical Society* **142**, 18936–18945 (2020).
- ⁴⁷R. Benn, H. Michael B  ch, and R.-D. Reinhardt, "Heavy metal spin- $\frac{1}{2}$ nuclei. Platinum-195 relaxation times in phosphorus-platinum(o) compounds and their dependence on the geometry of the complex," *Magnetic Resonance in Chemistry* **23**, 559–564 (1985).
- ⁴⁸A. Bagno and R. Bini, "NMR Spectra of Terminal Oxo Gold and Platinum Complexes: Relativistic DFT Predictions," *Angewandte Chemie International Edition* **49**, 1083–1086 (2010).
- ⁴⁹F. A. Perras, A. Venkatesh, M. P. Hanrahan, T. W. Goh, W. Huang, A. J. Rossini, and M. Pruski, "Indirect detection of infinite-speed MAS solid-state NMR spectra," *Journal of Magnetic Resonance* **276**, 95–102 (2017).
- ⁵⁰A. Venkatesh, M. J. Ryan, A. Biswas, K. C. Boteju, A. D. Sadow, and A. J. Rossini, "Enhancing the Sensitivity of Solid-State NMR Experiments with Very Low Gyromagnetic Ratio Nuclei with Fast Magic Angle Spinning and Proton Detection," *The Journal of Physical Chemistry A* **122**, 5635–5643 (2018).
- ⁵¹A. Venkatesh, D. Gioffr  , B. A. Atterberry, L. Rochlitz, S. L. Carnahan, Z. Wang, G. Menzildjian, A. Lesage, C. Cop  ret, and A. J. Rossini, "Molecular and Electronic Structure of Isolated Platinum Sites Enabled by the Expedient Measurement of 195Pt Chemical Shift Anisotropy," *Journal of the American Chemical Society* **144**, 13511–13525 (2022).
- ⁵²A. Venkatesh, F. A. Perras, and A. J. Rossini, "Proton-detected solid-state NMR spectroscopy of spin-1/2 nuclei with large chemical shift anisotropy," *Journal of Magnetic Resonance* **327**, 106983 (2021).
- ⁵³H. Adams, N. A. Bailey, B. E. Mann, B. F. Taylor, C. White, and P. Yavari, "Activation energies for molecular tumbling and cyclopentadienyl rotation in [M(H5-C5H5)(H4-cod)](M = Rh or Ir; cod = cyclo-octa-1,5-diene) and the X-ray crystal structure of and bonding in [Rh(H5-C5H5)(H4-cod)]," *Journal of the Chemical Society, Dalton Transactions*, 1947–1951 (1987).
- ⁵⁴B. L. Phillips, J. R. Houston, J. Feng, and W. H. Casey, "Observation of Solid-State 103Rh NMR by Cross-Polarization," *Journal of the American Chemical Society* **128**, 3912–3913 (2006).
- ⁵⁵G. L. Stoychev, A. A. Auer, R. Izs  k, and F. Neese, "Self-Consistent Field Calculation of Nuclear Magnetic Resonance Chemical Shielding Constants Using Gauge-Including Atomic Orbitals and Approximate Two-Electron Integrals," *Journal of Chemical Theory and Computation* **14**, 619–637 (2018).
- ⁵⁶G. L. Stoychev, A. A. Auer, and F. Neese, "Efficient and Accurate Prediction of Nuclear Magnetic Resonance Shielding Tensors with Double-Hybrid Density Functional Theory," *Journal of Chemical Theory and Computation* **14**, 4756–4771 (2018).
- ⁵⁷V. Barone and M. Cossi, "Quantum Calculation of Molecular Energies and Energy Gradients in Solution by a Conductor Solvent Model," *The Journal of Physical Chemistry A* **102**, 1995–2001 (1998).
- ⁵⁸M. Garcia-Rat  s and F. Neese, "Effect of the Solute Cavity on the Solvation Energy and its Derivatives within the Framework of the Gaussian Charge Scheme," *Journal of Computational Chemistry* **41**, 922–939 (2020).
- ⁵⁹R. Bouten, E. J. Baerends, E. van Lenthe, L. Visscher, G. Schreckenbach, and T. Ziegler, "Relativistic Effects for NMR Shielding Constants in Transition Metal Oxides Using the Zeroth-Order Regular Approximation," *The Journal of Physical Chemistry A* **104**, 5600–5611 (2000).
- ⁶⁰C. van W  llen, "Molecular density functional calculations in the regular relativistic approximation: Method, application to coinage metal diatomics, hydrides, fluorides and chlorides, and comparison with first-order relativistic calculations," *The Journal of Chemical Physics* **109**, 392–399 (1998).
- ⁶¹J. F. Dobson, "Alternative expressions for the Fermi hole curvature," *The Journal of Chemical Physics* **98**, 8870–8872 (1993).
- ⁶²S. Reimann, U. Ekstr  m, S. Stopkiewicz, A. M. Teale, A. Borgoo, and T. Helgaker, "The importance of current contributions to shielding constants in density-functional theory," *Physical Chemistry Chemical Physics* **17**, 18834–18842 (2015).
- ⁶³C. J. Schattenberg and M. Kaupp, "Effect of the Current Dependence of Tau-Dependent Exchange-Correlation Functionals on Nuclear Shielding Calculations," *Journal of Chemical Theory and Computation* **17**, 1469–1479 (2021).
- ⁶⁴F. Alkan and C. Dybowski, "Spin-orbit effects on the 125Te magnetic-shielding tensor: A cluster-based ZORA/DFT investigation," *Solid State Nuclear Magnetic Resonance* **95**, 6–11 (2018).
- ⁶⁵J. Autschbach, "The accuracy of hyperfine integrals in relativistic NMR computations based on the zeroth-order regular approximation," *Theoretical Chemistry Accounts* **112**, 52–57 (2004).
- ⁶⁶E. Malkin, S. Komorovsky, M. Repisky, T. B. Demissie, and K. Ruud, "The Absolute Shielding Constants of Heavy Nuclei: Resolving the Enigma of the 119Sn Absolute Shielding," *The Journal of Physical Chemistry Letters* **4**, 459–463 (2013).
- ⁶⁷R. Benn and A. Ruff  ska, "Indirect two-dimensional heteronuclear NMR spectroscopy of low-  metal nuclei (M = 183W, 57Fe, 103Rh, 61Ni)," *Magnetic Resonance in Chemistry* **26**, 895–902 (1988).
- ⁶⁸H. C. E. McFarlane, W. McFarlane, and D. S. Rycroft, "Studies of tungsten-183 magnetic shielding by heteronuclear magnetic double and triple resonance," *Journal of the Chemical Society, Dalton Transactions*, 1616–1622 (1976).
- ⁶⁹S. Weske, Y. Li, S. Wiegmann, and M. John, "H(C)Ag: A triple resonance NMR experiment for 109Ag detection in labile silver-carbene complexes," *Magnetic Resonance in Chemistry* **53**, 291–294 (2015).

The ^{103}Rh NMR Spectroscopy and Relaxometry of the Rhodium Formate Paddlewheel Complex

Harry Harbor-Collins¹, Mohamed Sabba¹, Gamal Moustafa¹,
Bonifac Legrady¹, Murari Soundararajan¹, Markus Leutzsch², and
Malcolm H. Levitt^{1,a}

¹School of Chemistry, University of Southampton, SO17 1BJ, UK

²Max-Planck-Institut für Kohlenforschung, Kaiser-Wilhelm-Platz
1, Mülheim an der Ruhr, 45470, Germany

July 25, 2023

^a Electronic mail: mhl@soton.ac.uk

1 Rhodium formate ^{13}C T_1

1.1 Pulse sequence

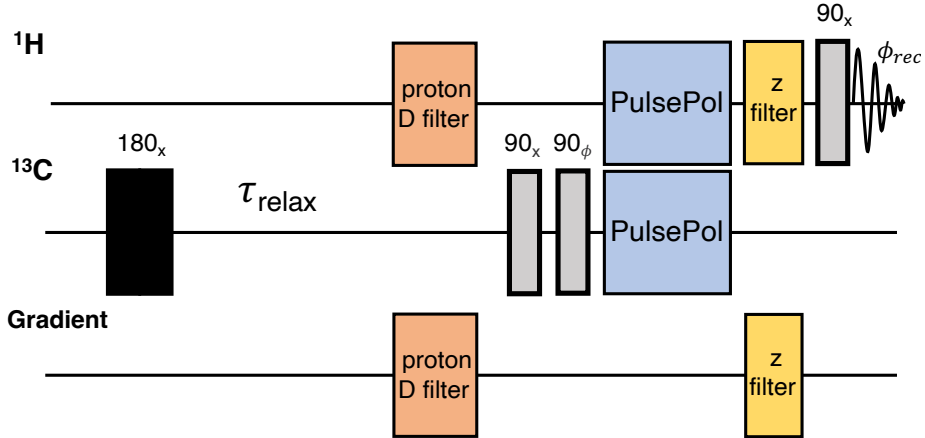


Figure S1: Sequence used for the indirect measurement of carbon T_1 through ^1H NMR signals. Phase cycles are given by $\phi = [-x, x]$ and the receiver $\phi_{\text{rec}} = [x, -x]$.

^{13}C T_1 relaxation time constants were measured indirectly through ^1H NMR signals using the sequence shown in figure S1. Longitudinal ^{13}C magnetisation is inverted by an initial 180° pulse, and allowed to relax towards equilibrium during the waiting interval τ_{relax} . A proton destruction filter is applied to eliminate any residual proton magnetisation generated during the waiting interval. Remaining ^{13}C z-magnetisation, selected for by the two 90° pulses, is now transferred back to ^1H z-magnetisation by a DualPol block and is selected for by a proton z-filter. A final ^1H 90° pulse generates observable ^1H transverse magnetization. The sequence is repeated with variation of the waiting interval τ_{relax} in order to follow the equilibration of longitudinal ^{13}C magnetization.

1.2 Rhodium formate ^{13}C T_1 decay curve

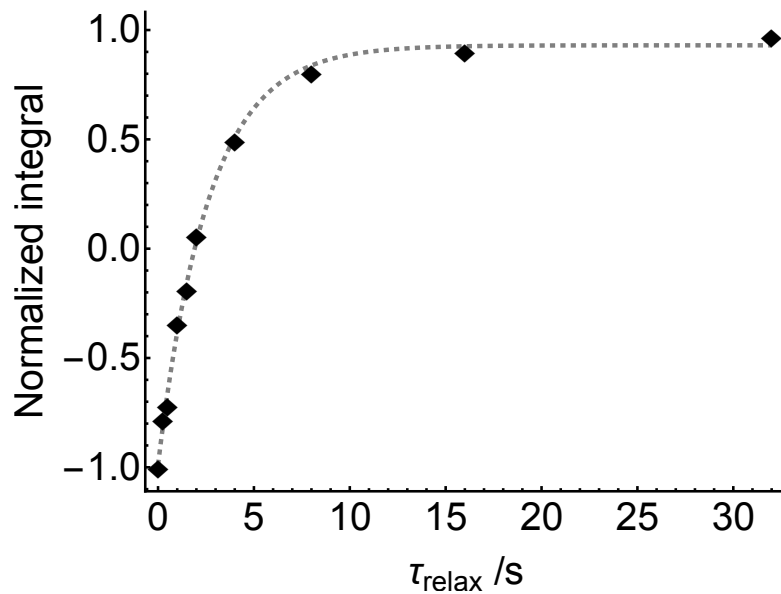


Figure S2: Experimental ^{13}C longitudinal magnetization recovery for rhodium formate dissolved in THF-d_8 at a field of 9.4 T. The integrals are normalised against the first data point.

The trajectory of indirectly-detected ^{13}C z-magnetization in a field of 9.4 T is shown in figure S2. The trajectory fits well to a single-exponential decay with a time constant of 2.64 ± 0.13 seconds.

2 Quantum chemical calculations

2.1 Geometry optimisation

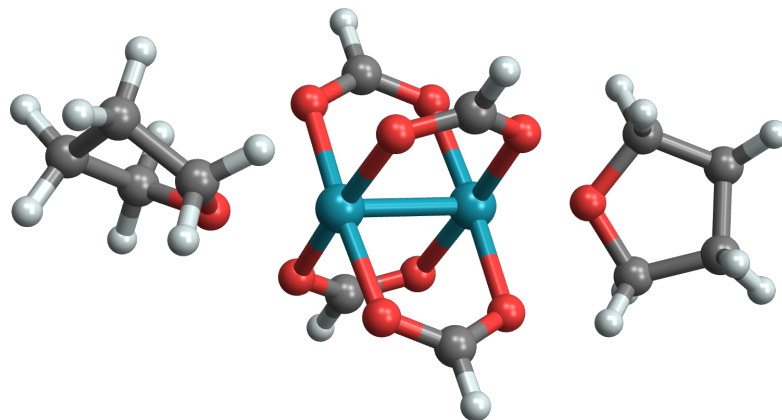


Figure S3: Rhodium formate with axial ligation by THF molecules geometry optimised structure.

The geometry of the rhodium formate complex axially ligated by solvent THF molecules was optimised using the ORCA program package version 5.0.3 [?]. Calculations were performed at the B3LYP/SARC-ZORA-TZVP level of theory. The .xyz file describing the optimized molecular coordinates is provided separately with the supplement.

2.2 Shielding tensor calculation

The ^{103}Rh shielding tensors were computed at the TPSSh/SARC-ZORA-TZVPP level of theory using implicit solvation (CPCM[?, ?] for THF), the zeroth-order regular approximation (ZORA)[?, ?] for the inclusion of relativistic effects, GIAOs, the RI approximation[?] and the tau-dependent correction as suggested by Dobson[?, ?, ?]. The full ORCA input files and output files for the calculation are provided separately in the supplement.

SARC-ZORA-def2-TZVPP							
Nucleus 0Rh:				Nucleus 1Rh:			
Diamagnetic contribution to the shielding tensor (ppm) :				Diamagnetic contribution to the shielding tensor (ppm) :			
	4410.161	0.086	-2.756		4410.086	-0.794	-2.536
	0.495	4433.006	2.014		-2.520	4430.981	-2.178
	-4.584	1.735	4429.880		-4.256	-2.188	4432.102
Paramagnetic contribution to the shielding tensor (ppm):				Paramagnetic contribution to the shielding tensor (ppm):			
	-17017.333	-15.541	-906.188		-17027.684	-106.738	-917.290
	-36.835	-10055.868	76.951		-35.853	-10182.105	-25.233
	-895.045	89.592	-10251.484		-907.773	-51.614	-10141.497
Total shielding tensor (ppm):				Total shielding tensor (ppm):			
	-12607.172	-15.454	-908.944		-12617.599	-107.532	-919.826
	-36.340	-5622.862	78.965		-38.373	-5751.124	-27.412
	-899.628	91.327	-5821.604		-912.029	-53.803	-5709.395

Figure S4: Output of the CSA calculations in ORCA.

2.3 Dipolar contributions to the ^{103}Rh $(T_1)^{-1}$

In the extreme narrowing limit, the contribution of a heteronuclear dipolar coupling to the ^{103}Rh $(T_1)^{-1}$ relaxation rate constant (when the heteronucleus is decoupled) is given by,

$$(T_1(^{103}\text{Rh}))_{\text{Rh}X}^{-1} = b_{\text{Rh}X}^2 \tau_c \quad (\text{S1})$$

Where $b_{\text{Rh}X}$ represents the dipolar coupling constant between the ^{103}Rh and the heteronucleus X and τ_c is the rotational correlation time. In contrast, the contribution of the homonuclear ^{103}Rh dipolar coupling to the ^{103}Rh $(T_1)^{-1}$ relaxation rate constant is given by,

$$(T_1(^{103}\text{Rh}))_{\text{RhRh}}^{-1} = \frac{3}{2} b_{\text{RhRh}}^2 \tau_c \quad (\text{S2})$$

Where $b_{\text{Rh}X}$ represents the dipolar coupling constant between the ^{103}Rh nuclei and τ_c is again the rotational correlation time. Using the optimised geometry in figure S3, the ^{103}Rh - ^1H dipolar coupling was estimated to be $\sim 2\pi$ 61 Hz; whereas the ^{103}Rh - ^{103}Rh homonuclear dipolar coupling constant was estimated to be $\sim 2\pi$ 8 Hz. These are extremely small numbers - the $^{103}\text{Rh}(T_1)$ resulting purely from the dipolar mechanism is predicted to be on the order of a day.

3 Solid-state NMR

3.1 Solid-state ^{13}C spectra

Solid-state ^{13}C spectra were straightforward to acquire at 14.1 T using a packed 4 mm rotor (~ 15 mg of sample). The pulse sequence used to acquire the solid-state ^{13}C spectra that appear in the main text is illustrated below.

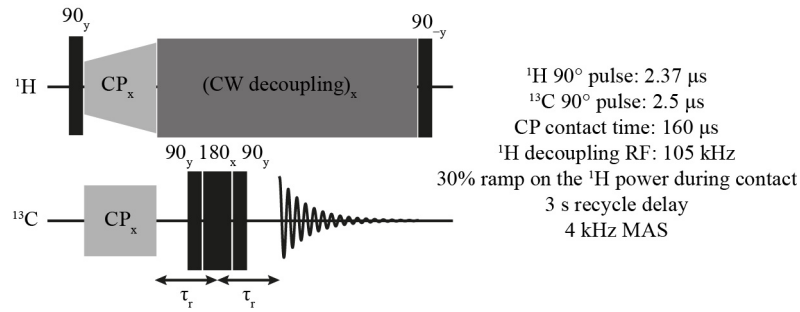


Figure S5: Sequence used for the measurement of the ^{13}C CPMAS spectra that appear in the main text. All of the relevant experimental parameters are illustrated in the figure.